Electronic Supplementary Information (ESI)

Effective methods to the synthesis of hydrazones, quinazolines, and Schiff bases – reaction monitoring using chemometric approach

Jana Pisk, Ivica Đilović, Tomica Hrenar, Danijela Cvijanović, Gordana Pavlović, and Višnja Vrdoljak*

Contents:

* *University of Zagreb, Faculty of Science, Department of Chemistry, Horvatovac 102a, 10000 Zagreb, Croatia; E-mail: visnja.vrdoljak@chem.pmf.hr.*

Table S1. General and crystal data, a summary of intensity data collection and structure refinement for the compounds: **1a·MeOH**, **1b·H₂O**, **3a**, **3b**, **3c·MeOH**, **4a**, **4b·MeOH**, **4c**, and **5b·H₂O**.

Identification code	1a·MeOH	1b·H₂O	3a	3b	3c·MeOH	4a	4b·MeOH	4c	5b·H₂O
Empirical formula	$C_{14}H_{15}N_3O_4$	$C_{13}H_{13}N_3O_4$	$C_{14}H_{13}N_3O_3$	$C_{14}H_{13}N_3O_3$	$C_{22}H_{21}N_3O_6$	$C_{14}H_{13}N_3O_3$	$C_{15}H_{17}N_3O_4$	$C_{21}H_{17}N_3O_5$	$C_{14}H_{14}N_2O_5$
M_r	289.29	275.26	271.27	271.27	423.42	271.27	303.32	391.38	290.27
T/K	150	293	293	293	293	293	150	293	293
Crystal system	monoclinic	monoclinic	orthorhombic	monoclinic	monoclinic	monoclinic	monoclinic	monoclinic	monoclinic
Space group	$P2_1/n$	$P2_1/n$	$Pbca$	$P2_1/n$	$C2/c$	$P2_1/c$	$P2_1/c$	$C2/c$	$P2_1/c$
a/Å	8.4964(4)	8.3319(3)	24.7572(13)	6.5511(6)	15.8673(7)	24.7095(14)	9.788(2)	39.4655(16)	15.2515(4)
b/Å	14.0972(6)	12.7546(6)	7.6282(5)	22.351(3)	10.0421(4)	10.1996(7)	8.4727(10)	5.4865(3)	6.7577(2)
c/Å	11.1992(5)	12.3732(7)	13.3499(6)	9.0707(12)	24.2618(12)	20.7620(14)	18.273(3)	16.4148(7)	13.2137(3)
α/°	90	90	90	90	90	90	90	90	90
β/°	95.924(4)	99.089(4)	90	97.757(11)	91.637(4)	99.252(5)	103.86(2)	95.157(4)	101.876(2)
γ/°	90	90	90	90	90	90	90	90	90
V/Å³	1334.23(10)	1298.39(11)	2521.2(2)	1316.0(3)	3864.3(3)	5164.5(6)	1471.3(5)	3539.9(3)	1332.72(6)
Z	4	4	8	4	8	16	4	8	4
ρ_{calc}/g cm⁻³	1.440	1.408	1.429	1.369	1.456	1.396	1.369	1.469	1.447
μ/mm⁻¹	0.108	0.107	0.103	0.099	0.108	0.101	0.101	0.890	0.941
$F(000)$	608.0	576.0	1136.0	568.0	1776.0	2272.0	640.0	1632.0	608.00
Crystal size/mm³	0.23 × 0.22 × 0.11	0.33 × 0.27 × 0.11	0.3 × 0.2 × 0.05	0.63 × 0.25 × 0.12	0.22 × 0.22 × 0.18	0.67 × 0.42 × 0.15	0.16 × 0.13 × 0.04	0.22 × 0.16 × 0.03	0.49 × 0.4 × 0.17
2θ range/°	8.59 to 51.00	8.30 to 51.00	8.28 to 50.00	8.33 to 50.98	8.29 to 51.99	8.39 to 51.00	8.49 to 50.99	9 to 133.99	5.92 to 133.99
Index ranges	-10 ≤ h ≤ 10, -17 ≤ k ≤ 17, -13 ≤ l ≤ 13	-10 ≤ h ≤ 8, -15 ≤ k ≤ 7, -14 ≤ l ≤ 11	-27 ≤ h ≤ 29, -9 ≤ k ≤ 9, -14 ≤ l ≤ 15	-7 ≤ h ≤ 7, -24 ≤ k ≤ 27, -10 ≤ l ≤ 10	-19 ≤ h ≤ 10, -12 ≤ k ≤ 9, -29 ≤ l ≤ 29	-28 ≤ h ≤ 29, -10 ≤ k ≤ 12, -25 ≤ l ≤ 24	-11 ≤ h ≤ 10, -10 ≤ k ≤ 10, -21 ≤ l ≤ 22	-43 ≤ h ≤ 46, -5 ≤ k ≤ 6, -19 ≤ l ≤ 19	-17 ≤ h ≤ 18, -8 ≤ k ≤ 7, -15 ≤ l ≤ 15
Reflections collected	45731	4884	7090	5134	7907	21864	7864	8028	5738
Independent reflections	2464 [R_{int} = 0.0522, R_{sigma} = 0.0195]	2403 [R_{int} = 0.0226, R_{sigma} = 0.0413]	2117 [R_{int} = 0.0492, R_{sigma} = 0.0862]	2427 [R_{int} = 0.0314, R_{sigma} = 0.0598]	3784 [R_{int} = 0.0256, R_{sigma} = 0.0431]	9550 [R_{int} = 0.0455, R_{sigma} = 0.0757]	2611 [R_{int} = 0.1118, R_{sigma} = 0.1727]	3157 [R_{int} = 0.0234, R_{sigma} = 0.0268]	2347 [R_{int} = 0.0210, R_{sigma} = 0.0205]
Data/restraints/parameters	2464/0/194	2403/0/191	2117/0/184	2427/0/184	3784/22/313	9550/0/733	2611/0/204	3157/0/266	2347/0/197
Goodness-of-fit on F^2	1.020	1.017	0.899	1.010	1.013	0.985	0.991	1.054	1.035
Final R indexes [$I{\geq}2\sigma(I)$]	R_1 = 0.0390, wR_2 = 0.1024	R_1 = 0.0461, wR_2 = 0.0895	R_1 = 0.0511, wR_2 = 0.0894	R_1 = 0.0586, wR_2 = 0.1430	R_1 = 0.0595, wR_2 = 0.1282	R_1 = 0.0598, wR_2 = 0.1132	R_1 = 0.0815, wR_2 = 0.1226	R_1 = 0.0439, wR_2 = 0.1273	R_1 = 0.0499, wR_2 = 0.1444
Final R indexes [all data]	R_1 = 0.0477, wR_2 = 0.1083	R_1 = 0.0813, wR_2 = 0.1021	R_1 = 0.0986, wR_2 = 0.1052	R_1 = 0.1038, wR_2 = 0.1809	R_1 = 0.0927, wR_2 = 0.1445	R_1 = 0.1312, wR_2 = 0.1427	R_1 = 0.1854, wR_2 = 0.1578	R_1 = 0.0573, wR_2 = 0.1402	R_1 = 0.0549, wR_2 = 0.1531

*$R = \sum||F_o|-|F_c||/\sum F_o$, $w = 1/[\sigma^2(F_o^2)+(g_1P)^2+ g_2P]$ where $P = (F_o^2+2F_c^2)/3$, $S = \Sigma[w(F_o^2 - F_c^2)^2/(N_{obs} - N_{param})]^{1/2}$.

2b Crystal data for $C_{13}H_{11}N_3O_3$ ($M = 257.25$ g/mol): monoclinic, space group P2₁/n (no. 14), $a = 6.904(2)$ Å, $b = 24.922(5)$ Å, $c = 7.4482(11)$ Å, $\beta = 108.79(2)°$, $V = 1213.1(5)$ Å³, $Z = 4$, $T = 293(2)$ K, $\mu(MoK\alpha) = 0.103$ mm⁻¹, $D_{calc} = 1.408$ g/cm³, 1636 reflections measured ($8.554° \leq 2\Theta \leq 50.96°$), 1235 unique ($R_{int} = 0.0713$, $R_{sigma} = 0.0591$) which were used in all calculations. The final R_1 was 0.0746 (I > 2σ(I)) and wR_2 was 0.2619 (all data). Data collection was not completed due to problems with diffractometer. Model derived from the data is not sufficient for deposition nor publication (completeness is around 43%).
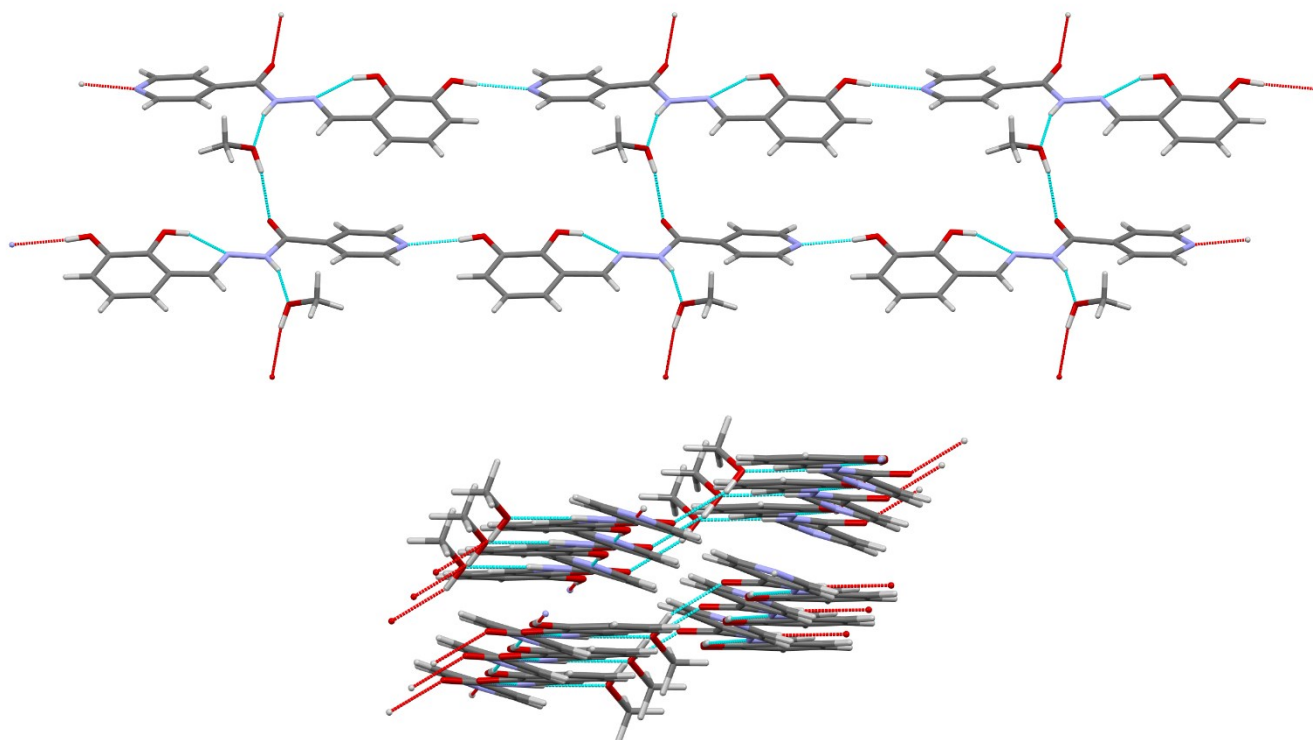
Figure S1. Crystal packing of compound **1a·MeOH**. Molecules of **1a** are arranged in arrays which are mutually connected with hydrogen bonds (MeOH molecules serve as a bridge) forming sheets. The view is projected down the crystallographic *a* axis (up). Sheets of molecules are held by stacking interactions (down).
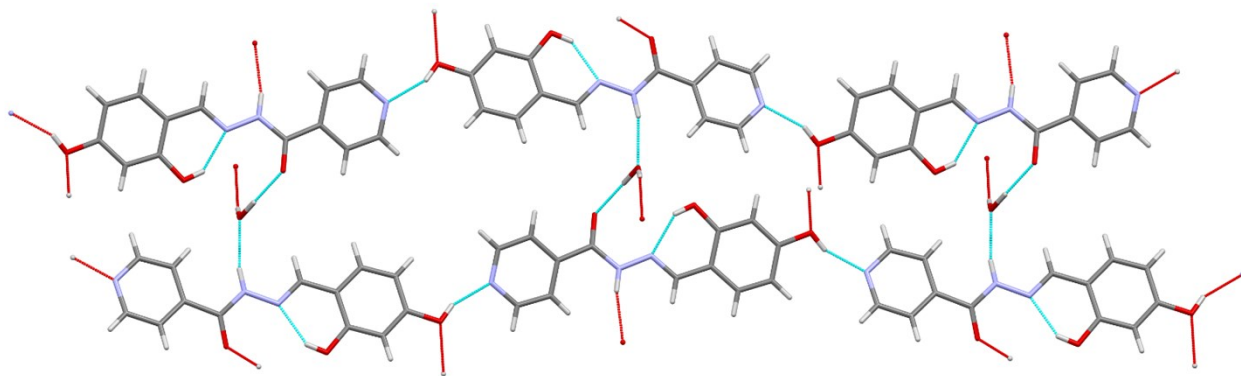
Figure S2. Crystal packing of compound **1b·H₂O**. Molecules of **1b** are arranged in arrays which are mutually connected with hydrogen bonds (water molecules serve as a bridge) forming sheets. The view is projected down the crystallographic *a* axis.
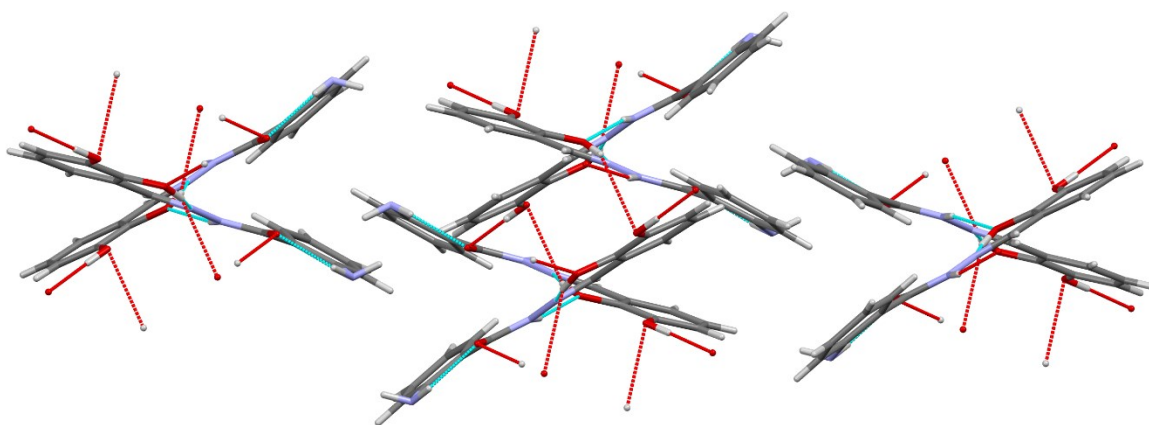
Figure S3. Crystal packing of compound **3a**. Molecules are connected with an extensive network of hydrogen bonds forming zig-zag like chains. The view is projected down the crystallographic *c* axis.
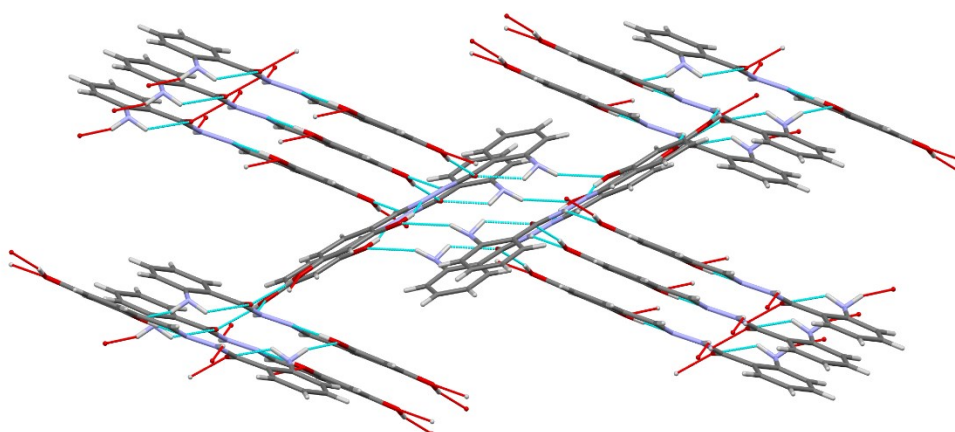
Figure S4. Crystal packing of compound **3b**. Molecules are connected with an extensive network of hydrogen bonds forming zig-zag like chains. The view is projected down the crystallographic *a* axis.
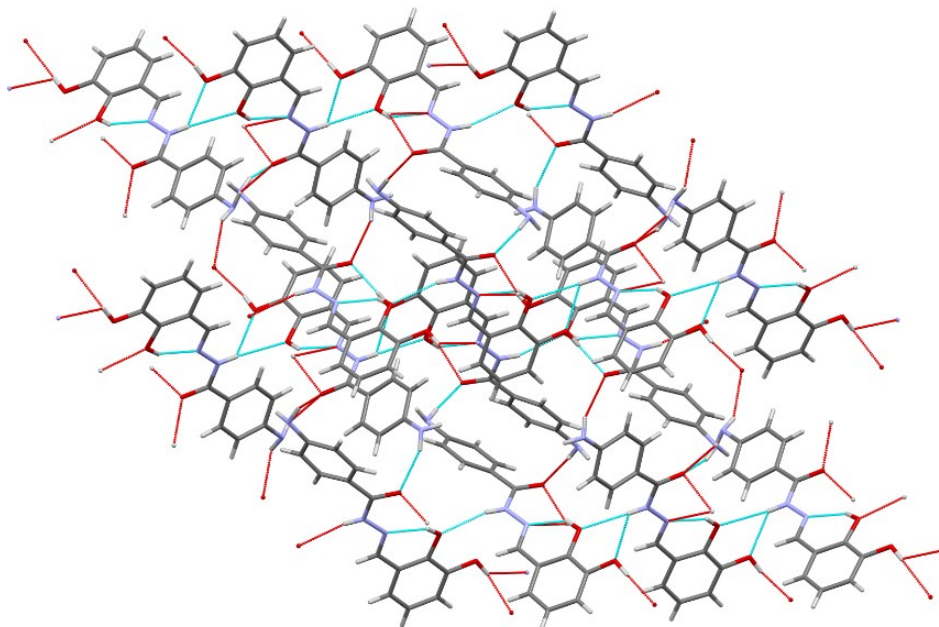
Figure S5. Crystal packing of compound **4a**. Molecules are connected with an extensive network of hydrogen bonds. The view is projected down the crystallographic *b* axis.

Figure S6. Crystal packing of compound **4b·MeOH**. Molecules are connected with an extensive network of hydrogen bonds. Methanol molecules serve as a bridge between sheets of hydrazone molecules. The view is projected down the crystallographic *c* axis.
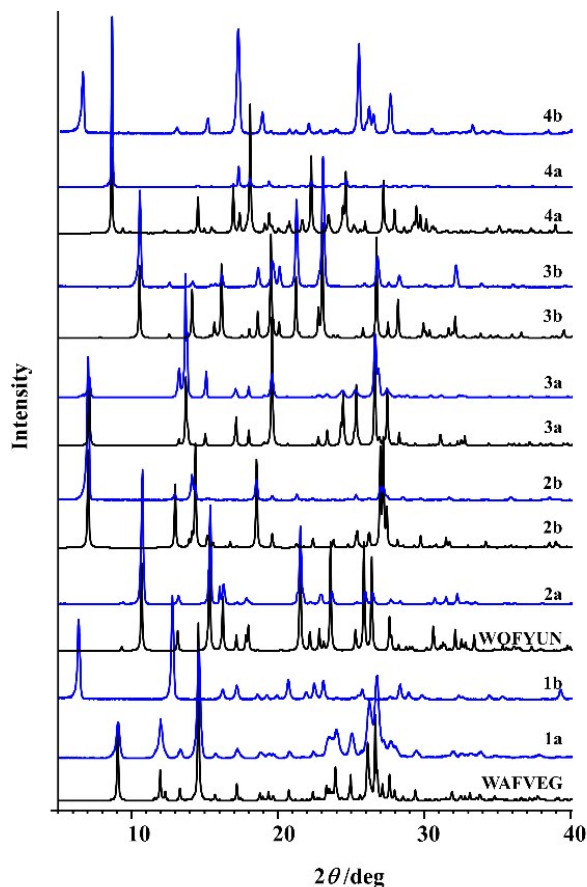
Figure S7. PXRD patterns of hydrazones obtained by the solution-based method. The blue lines indicate patterns obtained by powder diffraction, while the black lines indicate patterns calculated from the X-ray single-crystal structures of the corresponding non-solvated hydrazones.
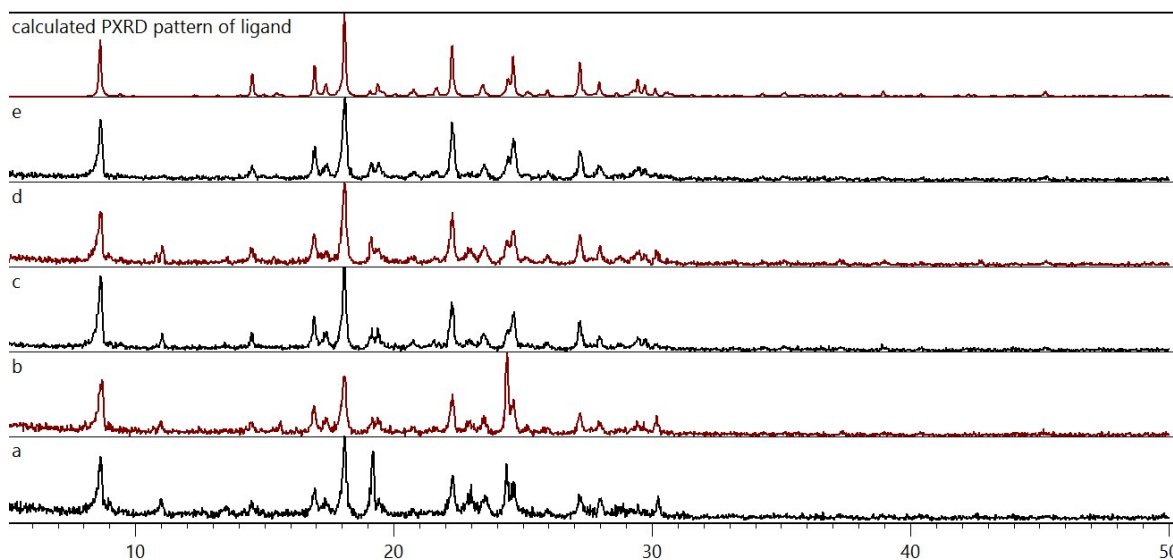
Figure S8. Comparison of the obtained PXRD patterns of samples taken at 10 min (a), 20 min (b), 30 min (c), 40 min (d), 60 min (e) of mechanochemical reaction with calculated PXRD pattern of **4a**.
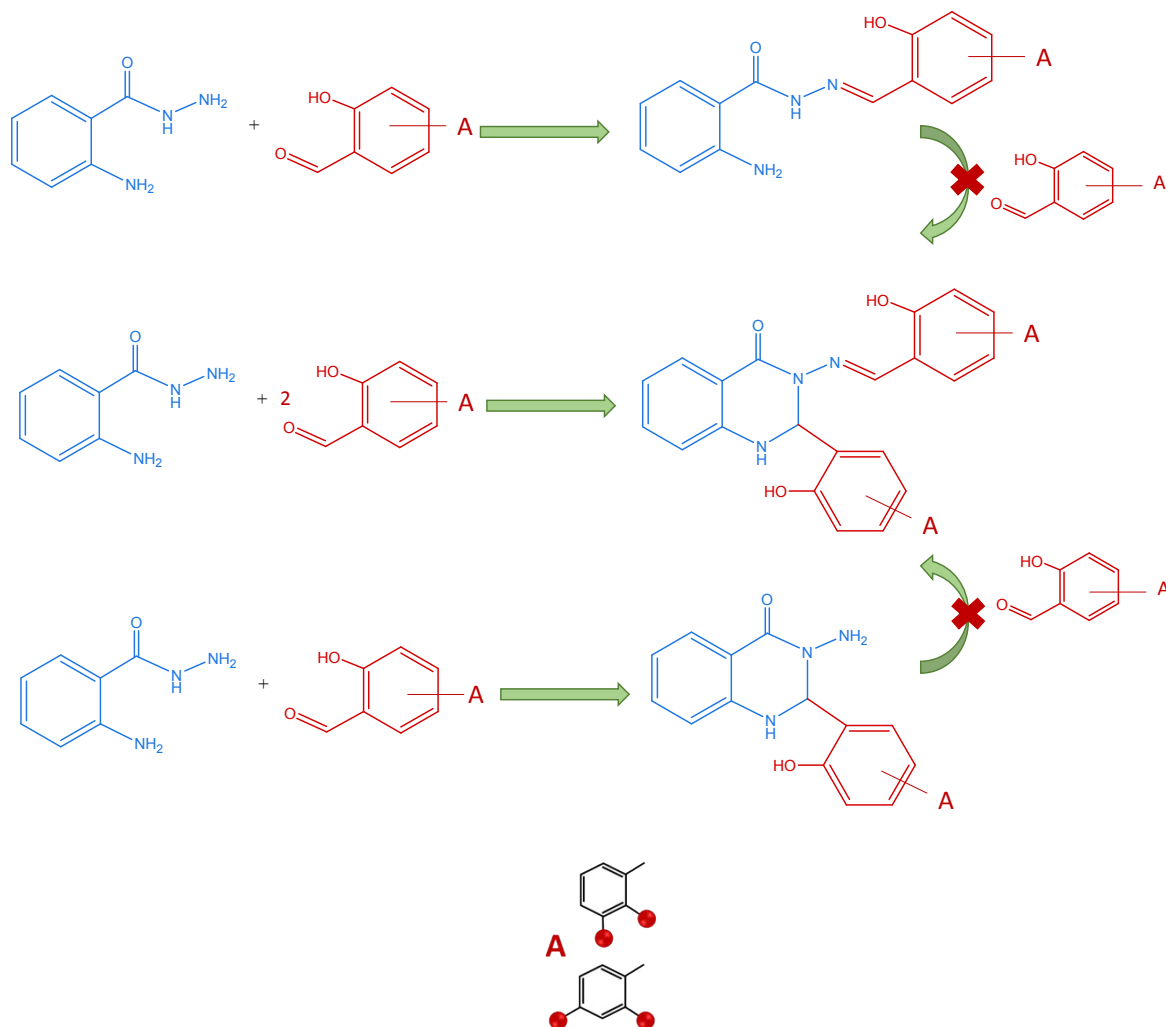
Scheme S1. Possible reactions of hydrazide and 2,3- or 2,4-dihydroxybenzaldehyde (from top to bottom): hydrazone formation; disubstituted quinazolin-4(3H)-one, and cyclic intermediate 3-amino-2-(2,4-dihydroxyphenyl)-4(3H)-quinazolinone.
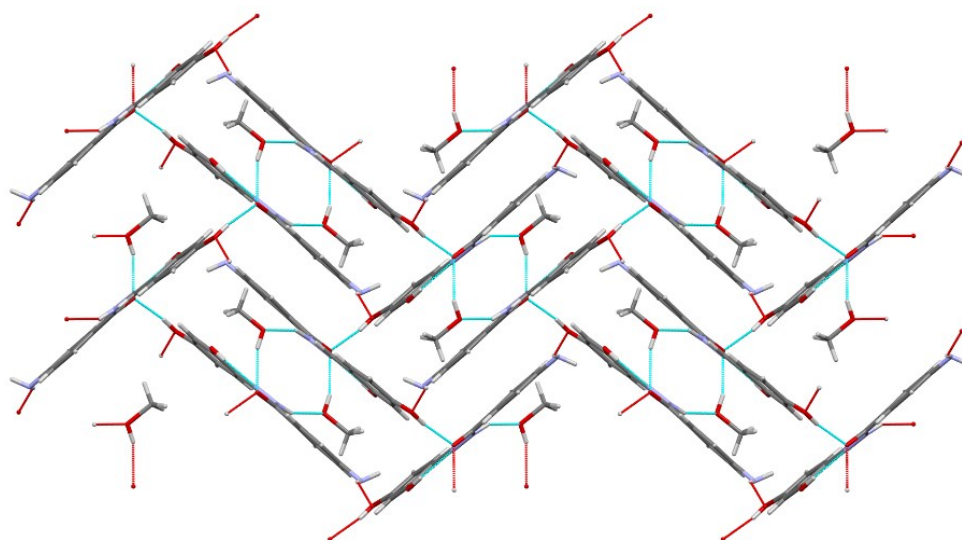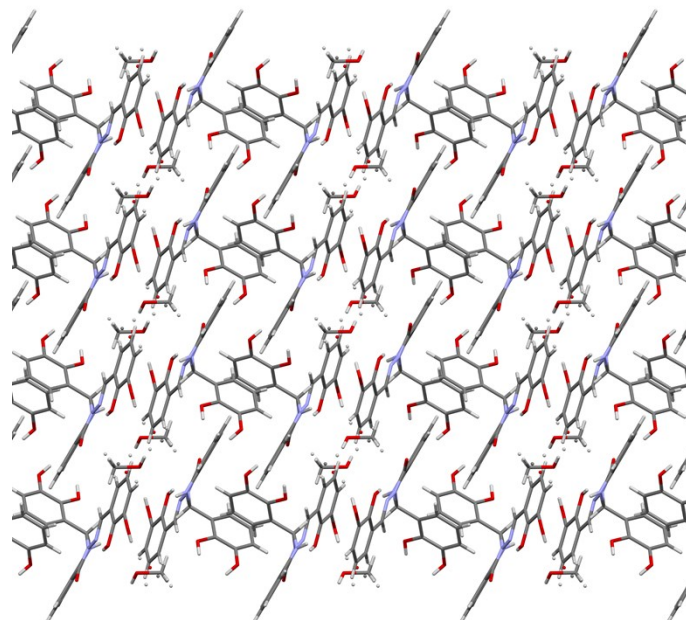
Figure S9. Crystal packing of compound **3c·MeOH**. Molecules are connected with an extensive network of hydrogen bonds. Disordered methanol molecules are found in the voids of so formed crystal structure (and held by hydrogen bonds). The view is projected down the crystallographic *b* axis.
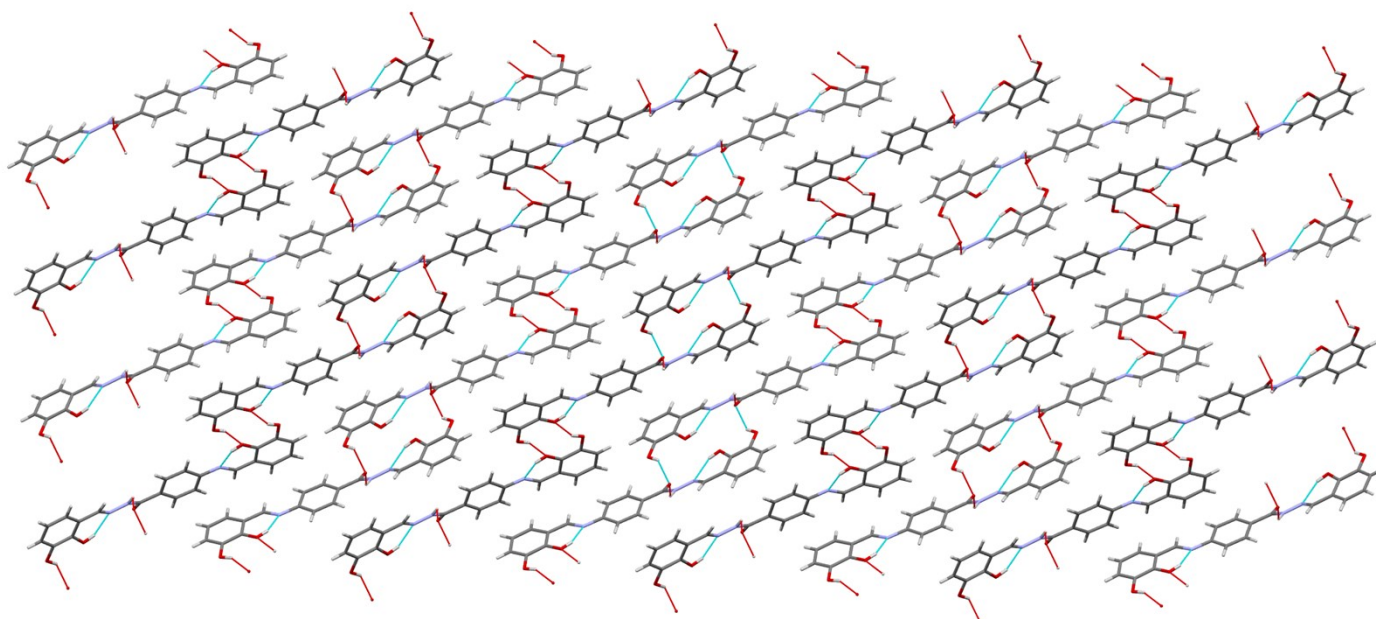

Figure S10. Crystal packing of compound **4c**. Molecules are connected with an extensive network of hydrogen bonds. The view is projected down the crystallographic *b* axis.

Analytical and selected IR spectral data

1a. IR: ($\tilde{v}_{max}$ / cm^{-1}): 3390 (O–H), 3082 (N–H), 2830 (C–H), 1679 (C=O), 1615 (N=C), 1557 (C=C)$_{ring}$, 1289, 1270 (C–O$_{phenyl}$), 1062 (N–N). Anal. calcd. for $C_{13}H_{11}N_3O_3$ (257.25): C, 60.69; H, 4.31; N, 16.34%. Found: C, 60.33; H, 4.11; N, 16.12%.

1b. IR: ($\tilde{v}_{max}$ / cm^{-1}): 3222 (O–H), 3085 (N–H), 2854 (C–H), 1643 (C=O), 1607 (N=C), 1583 (C=C)$_{ring}$, 1298, 1224 (C–O$_{phenyl}$), 1062 (N–N). Anal. calcd. for $C_{13}H_{11}N_3O_3$ (257.25): C, 60.69; H, 4.31; N, 16.34%. Found: C, 60.28; H, 4.05; N, 16.06%.

2a. IR: ($\tilde{v}_{max}$ / cm^{-1}): 3284 (O–H), 3066 (N–H), 2851 (C–H), 1668 (C=O), 1609 (N=C), 1548 (C=C)$_{ring}$, 1285, 1264 (C–O$_{phenyl}$), 1030 (N–N). Anal. calcd. for $C_{13}H_{11}N_3O_3$ (257.25): C, 60.69; H, 4.31; N, 16.34%. Found: C, 60.78; H, 4.12; N, 16.10%.

2b. IR: ($\tilde{v}_{max}$ / cm^{-1}): 3156 (O–H), 3066 (N–H), 2842 (C–H), 1633 (C=O), 1607 (N=C), 1575 (C=C)$_{ring}$, 1290, 1227 (C–O$_{phenyl}$), 1030 (N–N). Anal. calcd. for $C_{13}H_{11}N_3O_3$ (257.25): C, 60.69; H, 4.31; N, 16.34%. Found: C, 60.38; H, 4.14; N, 16.09%.

3a. IR: ($\tilde{v}_{max}$ / cm^{-1}): 3459 (O–H), 3337 (N–H), 3160 (H–C)$_{H-C=N}$, 1628 (C=O), 1616 (N=C), 1580, 1539 (C=C)$_{ring}$, 1266, 1243 (C–O$_{phenyl}$), 1163 (N–N). Anal. calcd. for $C_{14}H_{13}N_3O_3$ (271.27): C, 61.98; H, 4.83; N, 15.49%. Found: C, 61.78; H, 4.64; N, 15.17%.

3b. IR: ($\tilde{v}_{max}$ / cm^{-1}): 3471 (O–H), 3368 (N–H), 3073 (H–C)$_{H-C=N}$, 1633 (C=O), 1609 (N=C), 1578, 1545 (C=C)$_{ring}$, 1286, 1255 (C–O$_{phenyl}$), 1164 (N–N). Anal. calcd. for $C_{14}H_{13}N_3O_3$ (271.27): C, 61.98; H, 4.83; N, 15.49%. Found: C, 61.80; H, 4.76; N, 15.26%.

4a. IR: ($\tilde{v}_{max}$ / cm^{-1}): 3411 (O–H), 3258 (N–H), 3037 (H–C)$_{H-C=N}$, 1646 (C=O), 1603 (N=C), 1547 (C=C)$_{ring}$, 1285, 1262 (C–O$_{phenyl}$), 1176 (N–N). Anal. calcd. for $C_{14}H_{13}N_3O_3$ (271.27): C, 61.98; H, 4.83; N, 15.49%. Found: C, 61.83; H, 4.67; N, 15.22%.

4b. IR: ($\tilde{v}_{max}$ / cm^{-1}): 3492 (O–H), 3380 (N–H), 3198 (H–C)$_{H-C=N}$, 1620 (C=O), 1603 (N=C), 1562 (C=C)$_{ring}$, 1269 (C–O$_{phenyl}$), 1179 (N–N). Anal. calcd. for $C_{14}H_{13}N_3O_3$ (271.27): C, 61.98; H, 4.83; N, 15.49%. Found: C, 61.88; H, 4.69; N, 15.23%.

3c·MeOH. IR: ($\tilde{v}_{max}$ / cm^{-1}): 3380 (O–H), 1614 (N=C), 1506 (C=C)$_{ring}$, 1247 (C–O$_{phenyl}$), 1168 (N–N), 1022 (MeOH). Anal. calcd. for $C_{22}H_{21}N_3O_6$ (423.42): C, 62.40; H, 5.00; N, 9.93%. Found: C, 62.12; H, 4.79 ; N, 9.78%.

3d·MeOH. IR: ($\tilde{v}_{max}$ / cm^{-1}): 3227 (O–H), 1650 (C=O), 1609 (N=C), 1503 (C=C)$_{ring}$, 1220 (C–O$_{phenyl}$), 1168 (N–N), 1020 (MeOH). Anal. calcd. for $C_{22}H_{21}N_3O_6$ (423.42): C, 62.40; H, 5.00; N, 9.93%. Found: C, 62.14; H, 4.75; N, 9.72%.

4c. IR: ($\tilde{v}_{max}$ / cm^{-1}): 3227 (O–H), 1650 (C=O), 1620 (N=C), 1584 (C=C)$_{ring}$, 1223 (C–O$_{phenyl}$), 1150 (N–N). Anal. calcd. for $C_{21}H_{17}N_3O_5$ (391.38): C, 64.44; H, 4.38; N, 10.74%. Found: C, 64.35; H, 4.19; N, 10.88%.

4d. IR: ($\tilde{v}_{max}$ / cm^{-1}): 3227 (O–H), 1627 (C=O), 1594 (N=C), 1592 (C=C)$_{ring}$, 1220 (C–O$_{phenyl}$), 1168 (N–N). Anal. calcd. for $C_{21}H_{17}N_3O_5$ (391.38): C, 64.44; H, 4.38; N, 10.74%. Found: C, 64.45; H, 4.23; N, 10.62%.

5a. IR: ($\tilde{v}_{max}$ / cm^{-1}): 3481 (O–H), 1624 (C=O), 1588 (N=C), 1461 (C=C)$_{ring}$, 1267 (C–O$_{phenyl}$), 1153 (N–N). Anal. calcd. for $C_{14}H_{12}N_2O_4$ (272.26): C, 61.76; H, 4.44; N, 10.29%. Found: C, 61.53; H, 4.28; N, 10.01%.

5b. IR: ($\tilde{v}_{max}$ / cm^{-1}): 3240 (O–H), 1617 (C=O), 1589 (N=C), 1462 (C=C)$_{ring}$, 1240 (C–O$_{phenyl}$), 1120 (N–N). Anal. calcd. for $C_{14}H_{12}N_2O_4$ (272.26): C, 61.76; H, 4.44; N, 10.29%. Found: C, 61.54; H, 4.21; N, 9.95%.

Thermal behaviour

Hydrazones. DSC curves for the hydrazones **1a-4a**, **1b-4b**, show very similar patterns characterised by melting process accompanied with hydrazone decomposition. Melting onset is at 257 °C for **1a** ($\Delta_{fus}H$= 49.8 kJ/mol), 250 °C for **2a** ($\Delta_{fus}H$= 45.6 kJ/mol), 191 °C for **3a** ($\Delta_{fus}H$= 28.7 kJ/mol), 274 °C for **4a** ($\Delta_{fus}H$= 47.6 kJ/mol), 293 °C for **1b** ($\Delta_{fus}H$= 81.3 kJ/mol), 276 °C for **2b** ($\Delta_{fus}H$= 49.7 kJ/mol), 207 °C for **3b** ($\Delta_{fus}H$= 16.0 kJ/mol), 273 °C for **4b** ($\Delta_{fus}H$= 9.3 kJ/mol).

TG data for show only one mass loss at 281 °C for **1a**, 270 °C for **2a**, 213 °C for **3a**, 276 °C for **4a**, 279 °C for **1b**, 267 °C for **2b**, 214 °C for **3b**, and 280 °C for **4b**.

Quinazolin-4(3*H*)-ones. **3c·MeOH** and **3d·MeOH** show broad endothermic peak attributed to the methanol loss (for **3c·MeOH** onset is at 117 °C and for **3d·MeOH** around 71 °C), followed by the melting peak, at 170 °C for **3c·MeOH** ($\Delta_{fus}H$= 39.0 kJ/mol) and 150 °C for **3d·MeOH** ($\Delta_{fus}H$= 29.3kJ/mol). Moreover, TG data of the quinazolines **3c·MeOH** and **3d·MeOH** confirmed mass loss of methanol (7.1 % and 8.3 % (calcd. 7.6 %)) in the temperature range 123-154 °C and 82-103 °C, respectively. Afterwards the onset for the second mass loss for **3c·MeOH** is at 189 °C and for **3d·MeOH** at 266 °C.

Hidrazone-Schiff bases. DSC curves for **4c** and **4d**, as well show melting peak followed by endothermic decomposition, onset for **4c** is at 281 °C ($\Delta_{fus}H$= 53.4 kJ/mol), while for **4d** at 312 °C ($\Delta_{fus}H$= 62.7 kJ/mol).

Azines. DSC curves characteristic for **5a** and **5b** have very similar pattern, defined by very sharp and narrow melting peak at 261 °C for **5a** ($\Delta_{fus}H$= 56.9 kJ/mol) and 340 °C for **5b** ($\Delta_{fus}H$= 39.8 kJ/mol), followed by further decomposition of the compounds as confirmed by TG analysis.

NMR spectroscopy

Table S2 ^{1}H and ^{13}C chemical shifts (ppm) of **1a** and **1b**.

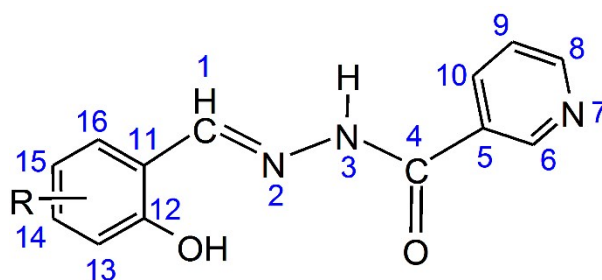| Atom	1a		1b	
	δ / ppm (^{1}H)	δ / ppm (^{13}C)	δ / ppm (^{1}H)	δ / ppm (^{13}C)
1	8.65	150.22	8.54	150.37
4	-	161.77	-	161.40
5	-	140.41	-	140.60
6	7.86	121.10	7.83	121.92
7	8.81	150.87	8.79	150.82
8	-	-	-	-
9	8.81	150.87	8.79	150.82
10	7.86	121.10	7.83	121.92
11	-	119.27	-	110.92
12	-	146.55	-	159.99
13	-	146.12	6.34	103.10
14	6.88	118.07	-	161.50
15	6.76	119.72	6.38	108.33
16	7.03	120.27	7.37	131.66
OH	9.31	-	10.01	-
	10.86	-	11.26	-
NH	12.31	-	12.12	-
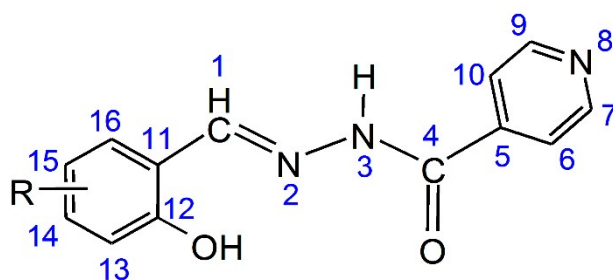
Figure S11. The structural formula of **1a** and **1b** with the NMR numbering scheme.

Table S3 ^{1}H and ^{13}C chemical shifts (ppm) of **2a** and **2b**.

Atom	2a		2b	
	δ / ppm (^{1}H)	δ / ppm (^{13}C)	δ / ppm (^{1}H)	δ / ppm (^{13}C)
1	8.62	149.80	8.52	149.96
4	-	161.87	-	161.53
5	-	129.13	-	129.30
6	9.10	149.09	9.08	149.01
7	-	-	-	-
8	8.79	152.94	8.77	152.77
9	7.60	124.13	7.58	124.09
10	8.29	135.94	8.26	135.83
11	-	119.25	-	110.93
12	-	146.60	-	159.97
13	-	146.10	6.34	103.11
14	6.88	117.99	-	161.38
15	6.75	119.69	6.38	108.27
16	7.02	120.36	7.36	131.71
OH	9.29	-	10.00	-
	10.96	-	11.33	-
NH	12.26	-	12.07	-

Figure S12. The structural formula of **2a** and **2b** with the NMR numbering scheme.
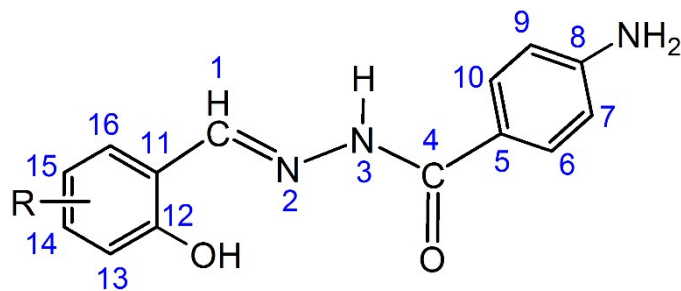
Table S4 ^{1}H and ^{13}C chemical shifts (ppm) of **3a** and **3b**.

| Atom	3a		3b	
	δ / ppm (^{1}H)	δ / ppm (^{13}C)	δ / ppm (^{1}H)	δ / ppm (^{13}C)
1	8.54	148.77	8.45	149.02
4	-	165.40	-	165.14
5	-	112.88	-	113.20
6	-	150.79	-	150.63
7	6.78	116.98	6.76	116.91
8	7.23	133.06	7.21	132.84
9	6.59	115.10	6.58	115.07
10	7.60	128.71	7.57	128.62
11	-	119.23	-	111.06
12	-	146.50	-	159.95
13	-	146.04	6.32	103.15
14	6.86	117.68	-	160.97
15	6.75	119.55	6.37	108.05
16	6.92	120.66	7.26	131.91
OH	9.16	-	9.94	-
	11.39	-	11.67	-
NH	11.88	-	11.67	-
NH$_2$	6.49	-	6.44	-
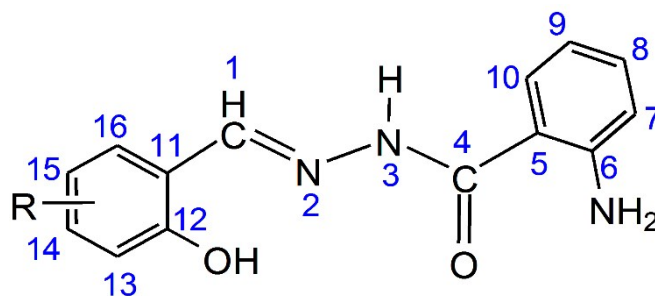
Figure S13. The structural formula of **3a** and **3b** with the NMR numbering scheme.

**Table S5** ^{1}H and ^{13}C chemical shifts (ppm) of **4a** and **4b**.

Atom	4a		4b	
	δ / ppm (^{1}H)	δ / ppm (^{13}C)	δ / ppm (^{1}H)	δ / ppm (^{13}C)
1	8.52	147.97	8.43	148.22
4	-	163.08	-	162.86
5	-	119.15	-	119.45
6	7.69	129.86	7.66	129.71
7	6.62	113.13	6.60	113.10
8	-	153.03	-	152.83
9	6.62	113.13	6.60	113.10
10	7.69	129.86	7.66	129.71
11	-	119.29	-	111.17
12	-	146.00	-	159.87
13	-	146.40	6.31	103.15
14	6.84	117.51	-	160.77
15	6.74	119.50	6.36	107.95
16	6.90	120.63	7.24	131.79
OH	9.12	-	9.90	-
	11.50	-	11.72	-
NH	11.74	-	11.54	-
NH$_2$	5.84	-	5.80	-

Figure S14. The structural formula of **4a** and **4b** with the NMR numbering scheme.
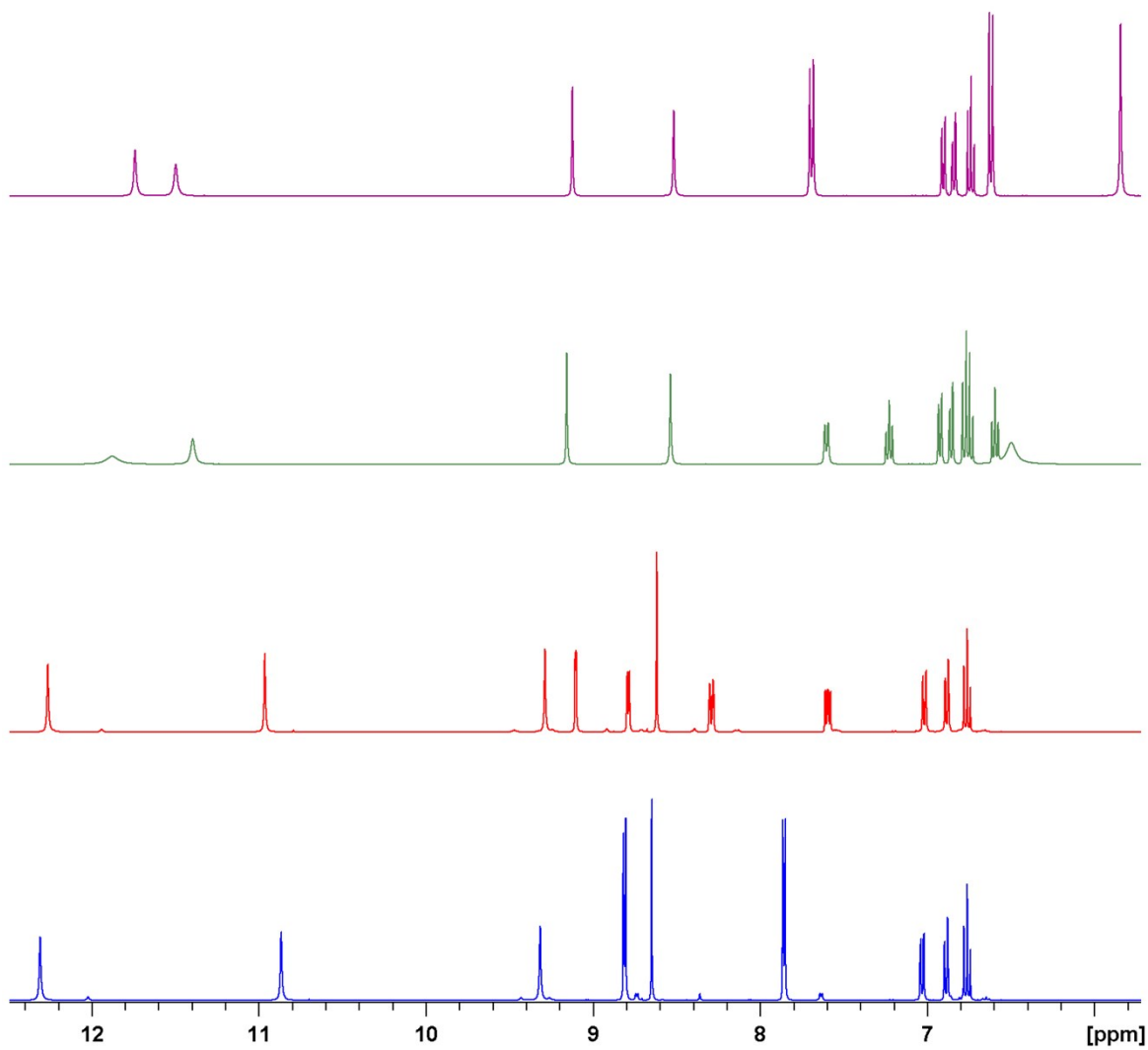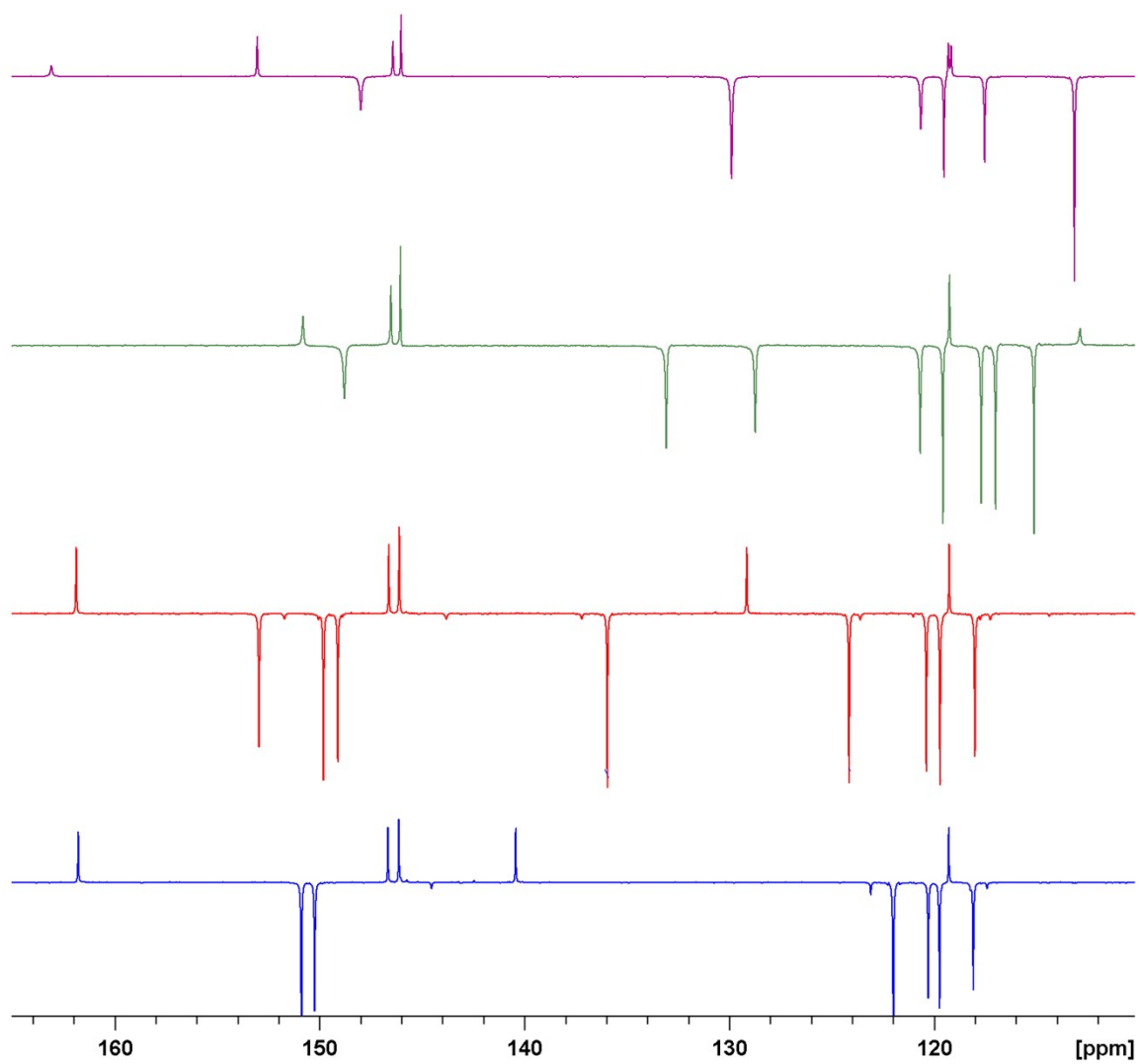
Figure S15. A portion of the ^{1}H NMR spectra in dmso-d_6 of: **1a**, **2a**, **3a**, and **4a** (from bottom to top).
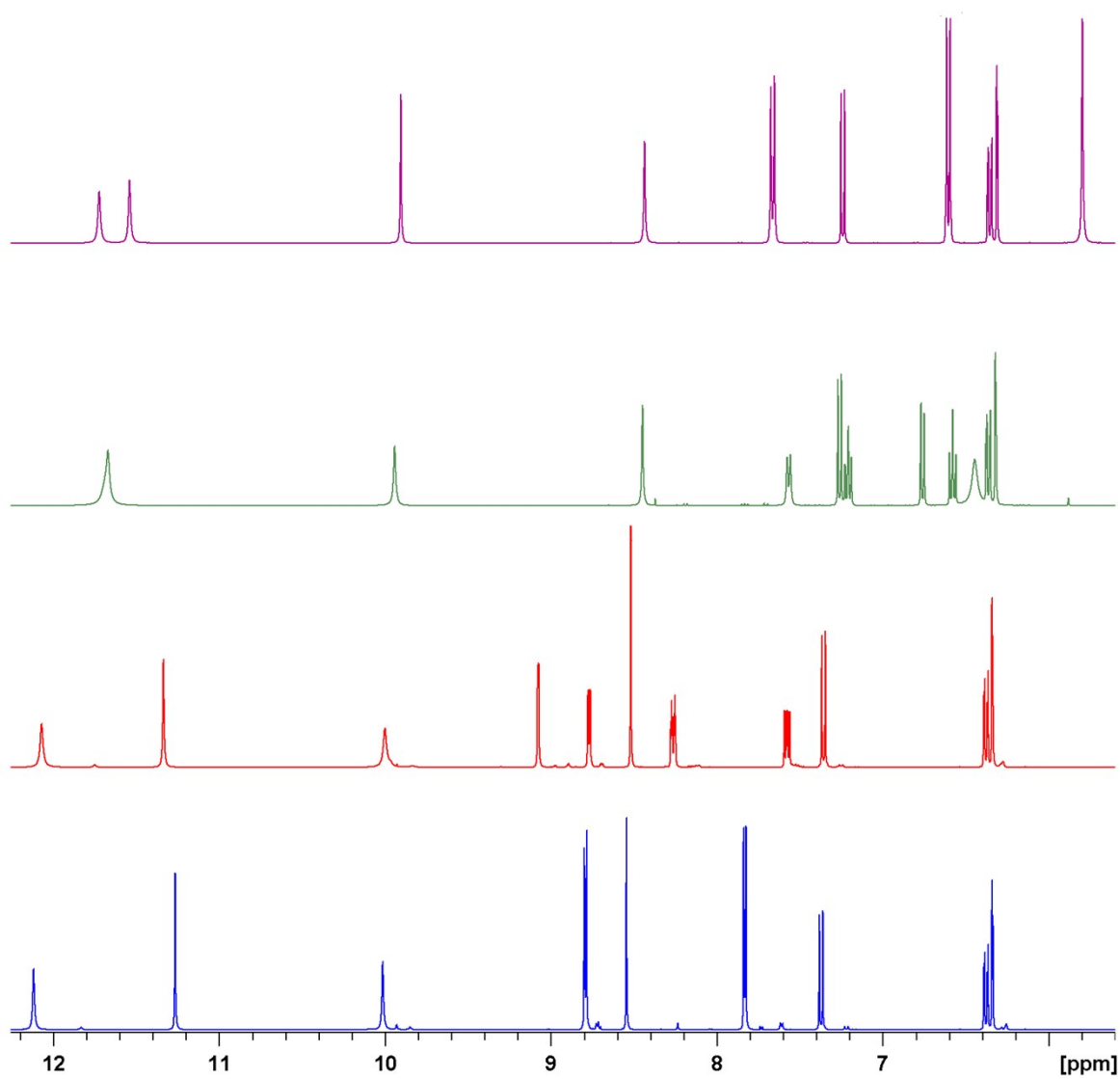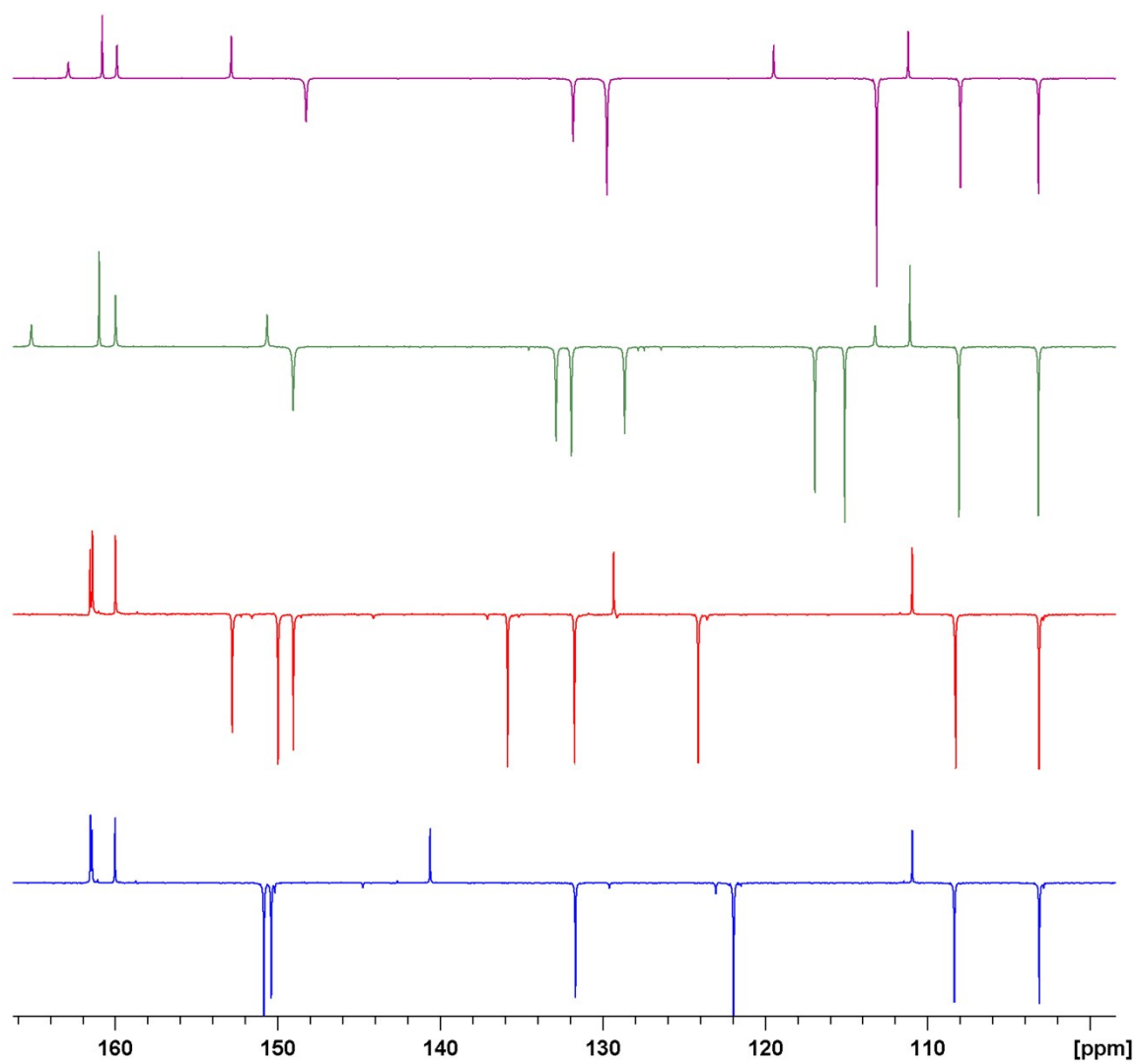
Figure S16. A portion of the ^{1}H NMR spectra in dmso-d_6 of: **1b**, **2b**, **3b**, and **4b** (from bottom to top).

Figure S17. A portion of the ^{13}C NMR spectra in dmso-d_6 of: **1a**, **2a**, **3a**, and **4a** (from bottom to top).

Figure S18. A portion of the ^{13}C NMR spectra in dmso-d_6 of: **1b**, **2b**, **3b**, and **4a** (from bottom to top).

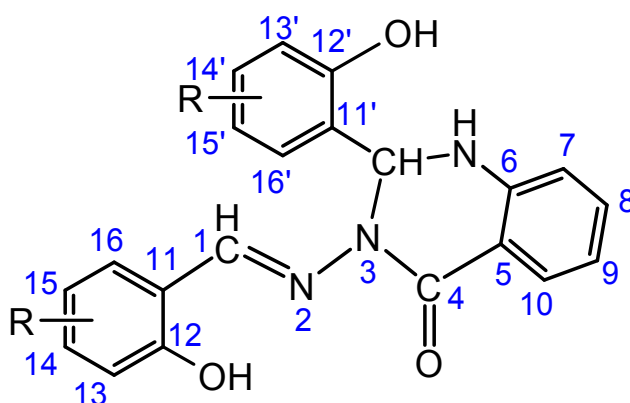**Table S6** [1]H and ^{13}C chemical shifts (ppm) of **3c** and **3d**.

| Atom	3c		3d	
	δ / ppm (^{1}H)	δ / ppm (^{13}C)	δ / ppm (^{1}H)	δ / ppm (^{13}C)
1	8.29	149.39	8.30	152.39
4	-	160.40	-	160.24
5	-	113.45	-	113.85
6	-	146.71	-	147.00
7	6.83	118.04	6.80	115.20
8	7.29	134.72	7.28	134.37
9	6.75	116.07	6.73	117.85
10	7.80	128.53	7.75	128.42
11	-	118.86	-	110.78
12	-	146.61	-	160.24
13	-	146.13	6.26	103.1
14	6.83	115.37	-	161.39
15	6.73	118.04	6.33	108.06
16	6.83	121.47	7.18	132.87
11'	-	125.68	-	115.81
12'	-	143.15	-	156.22
13'	-	145.98	6.35	103.1
14'	6.43	119.46	-	159.17
15'	6.51	119.55	6.10	106.83
16'	6.72	116.35	6.80	127.49
CH	6.87	65.45	6.61	66.24
OH	11.53 9.65 9.16 9.11	-	11.57 9.98 9.92 9.39	
NH	7.44	-	7.28	

Figure S19. The structural formula of **3c** and **3d** with the NMR numbering scheme.

Table S7 ^{1}H and ^{13}C chemical shifts (ppm) of **4c** and **4d**.

| Atom	4c		4d	
	δ / ppm (^{1}H)	δ / ppm (^{13}C)	δ / ppm (^{1}H)	δ / ppm (^{13}C)
1	8.63	149.46	8.53	149.56
4	-	162.57	-	162.31
5	-	131.12	-	130.66
6	8.07	129.58	8.01	129.43
7	7.58	121.98	7.49	121.65
8	-	151.63	-	151.69
9	7.58	121.98	7.49	121.65
10	8.07	129.58	8.01	129.43
11	-	119.17	-	111.04
12	-	146.58	-	159.99
13	-	146.08	6.33	103.15
14	6.88	119.80	-	161.18
15	6.76	119.65	6.38	108.17
16	6.99	120.55	7.32	131.84
1'	9.00	165.64	8.88	164.19
11'	-	119.26	-	112.55
12'	-	149.87	-	163.66
13'	-	146.15	6.33	102.87
14'	6.99	117.88	-	163.45
15'	6.83	119.45	6.44	108.65
16'	17.16	123.37	7.49	135.19
OH	12.86 11.18 9.29 9.23	-	13.32 11.52 10.37 9.97	-
NH	12.16	-	11.94	-
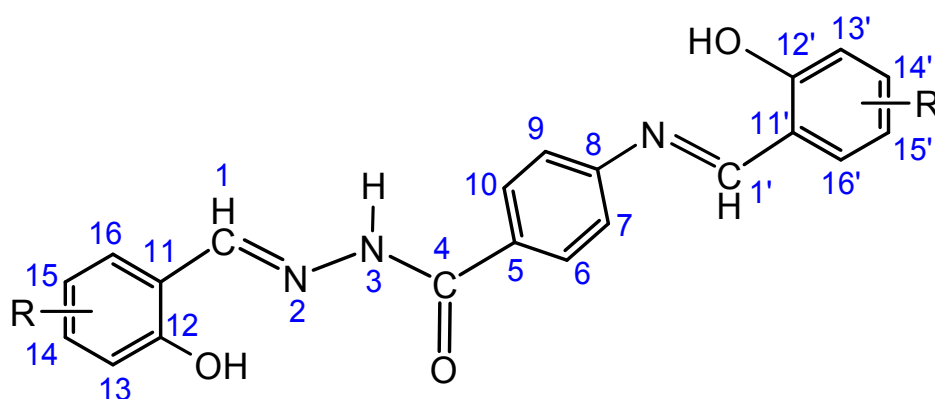
**Figure S20.** The structural formula of **4c** and **4d** with the NMR numbering scheme.
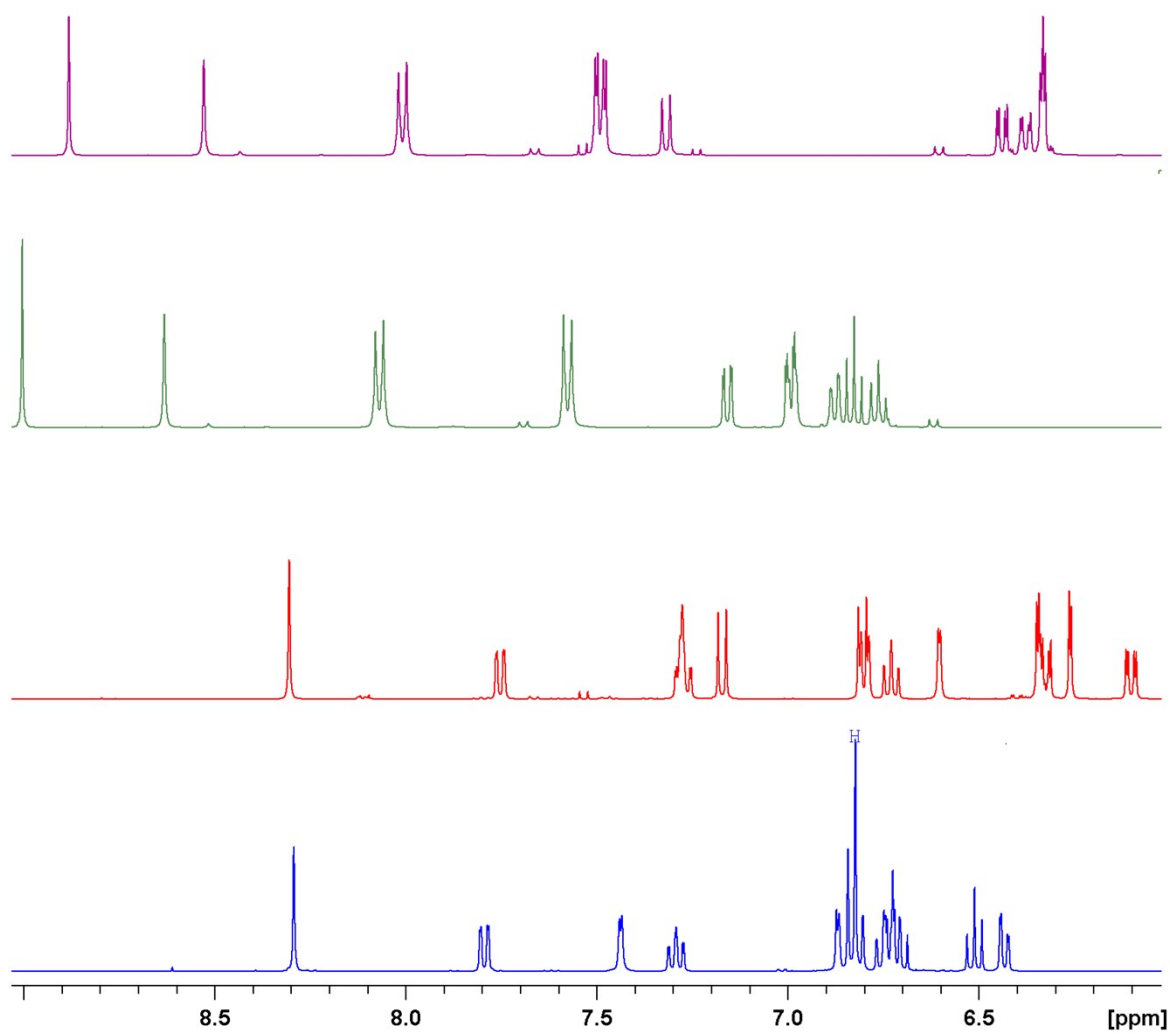
**Figure S21.** A portion of the ^{1}H NMR spectra in dmso-d_6 of: **3c**, **3d**, **4c**, and **4d** (from bottom to top).
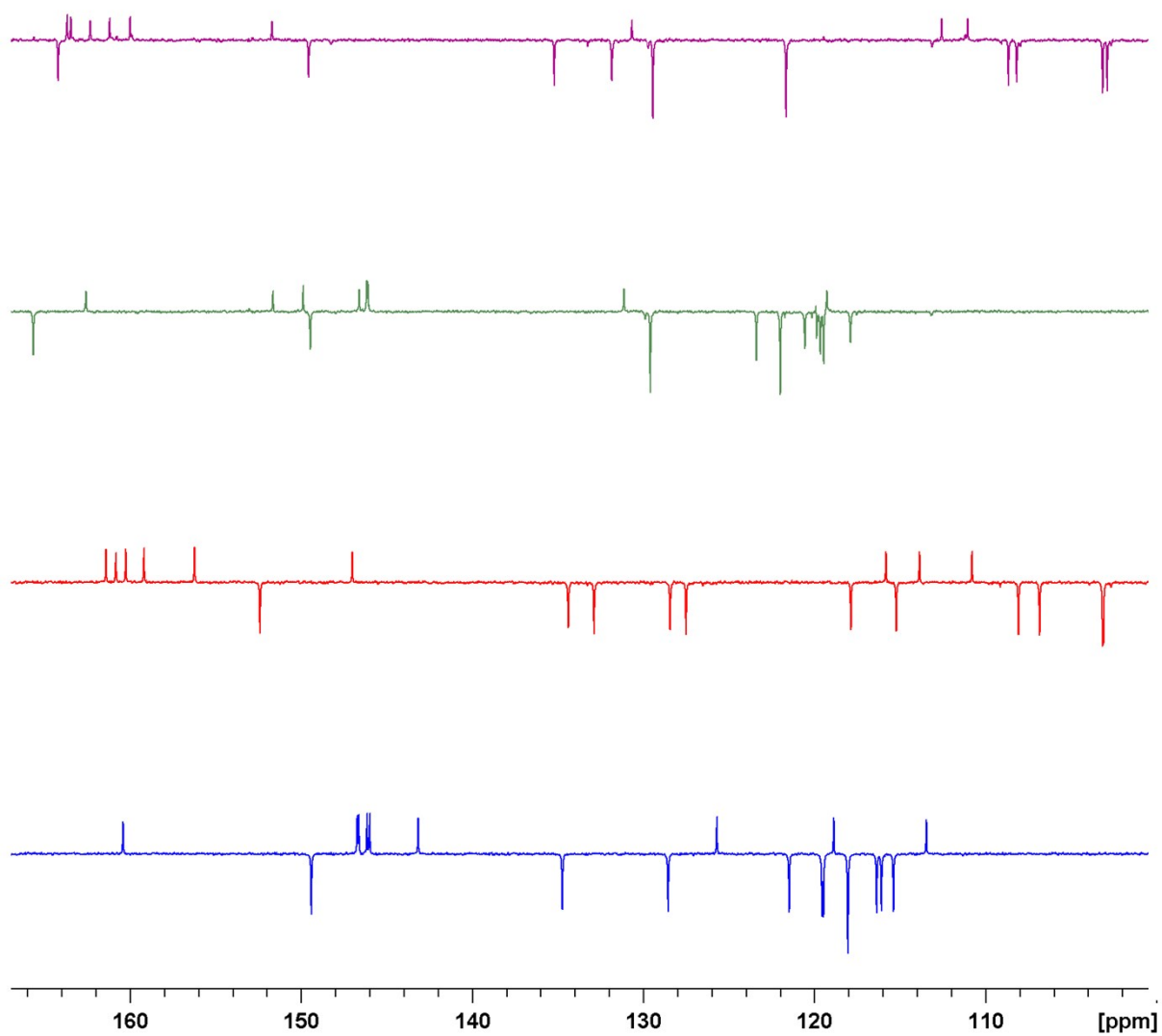
Figure S22. A portion of the ^{13}C NMR spectra in dmso-d_6 of: **3c**, **3d**, **4c**, and **4d** (from bottom to top).
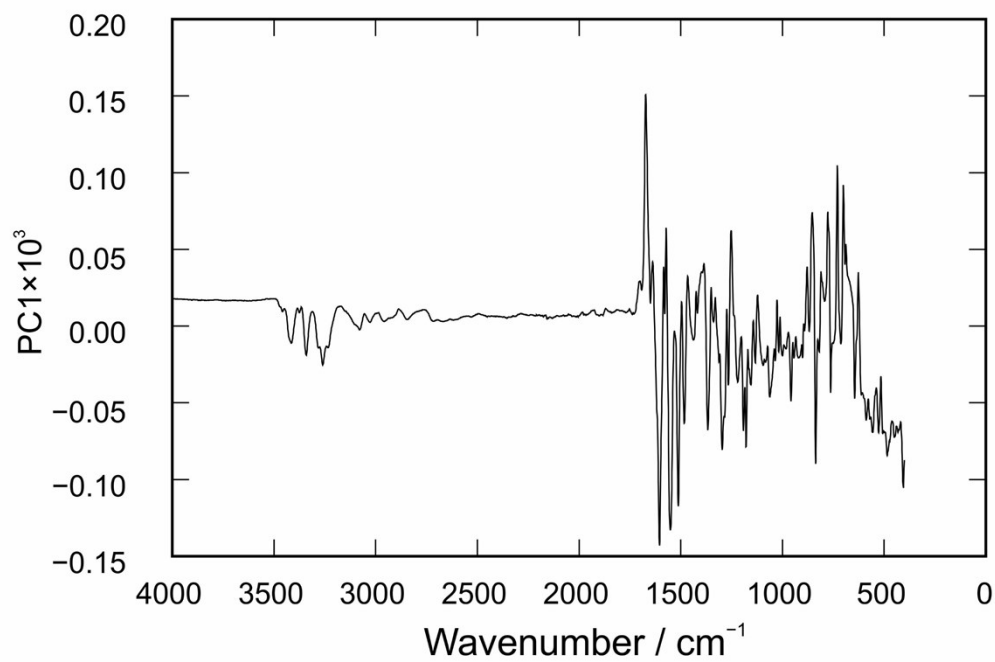
Figure S23. Principal component loadings calculated for a set of ATR spectra collected through vapour-mediated synthesis of **4a-3py.**
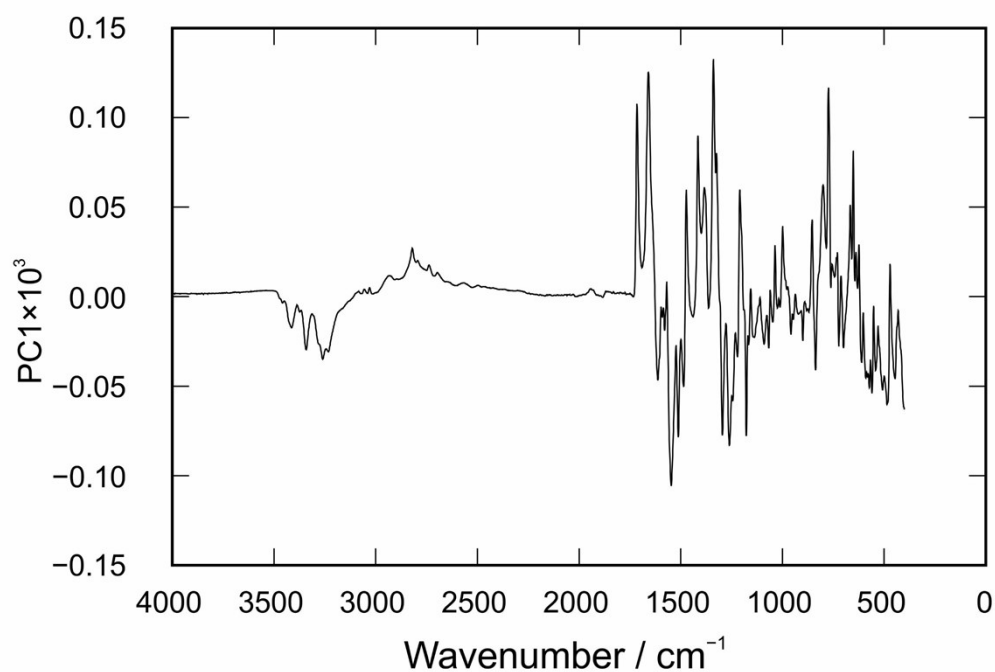
Figure S24. Principal component loadings calculated for a set of ATR spectra collected through vapour-mediated synthesis of **4a-4py.**
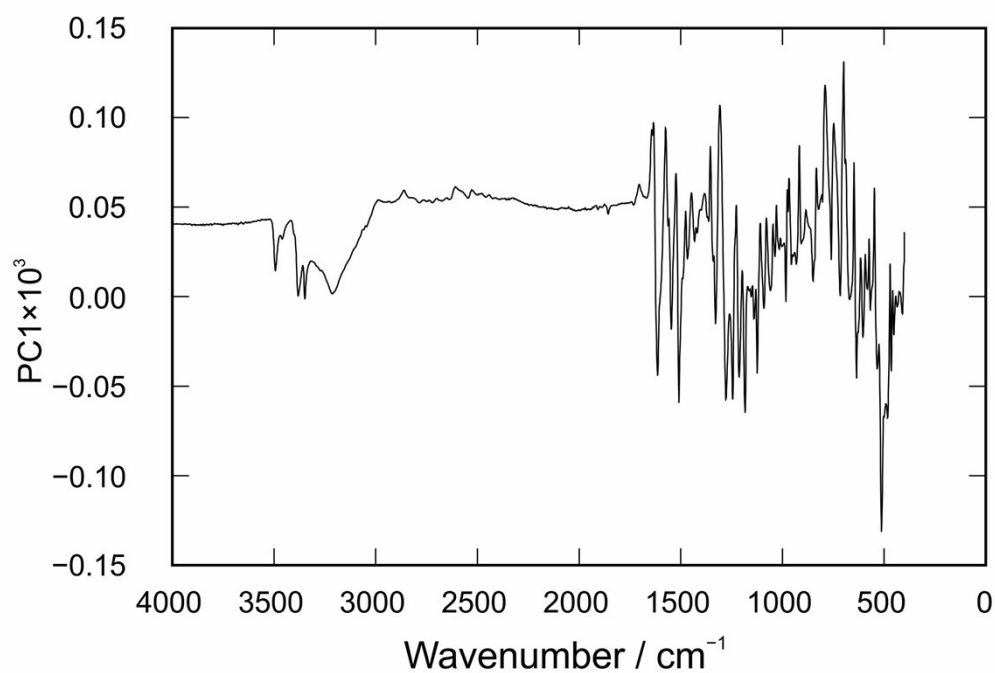
Figure S25. Principal component loadings calculated for a set of ATR spectra collected through vapour-mediated synthesis synthesis of **4b-3py.**
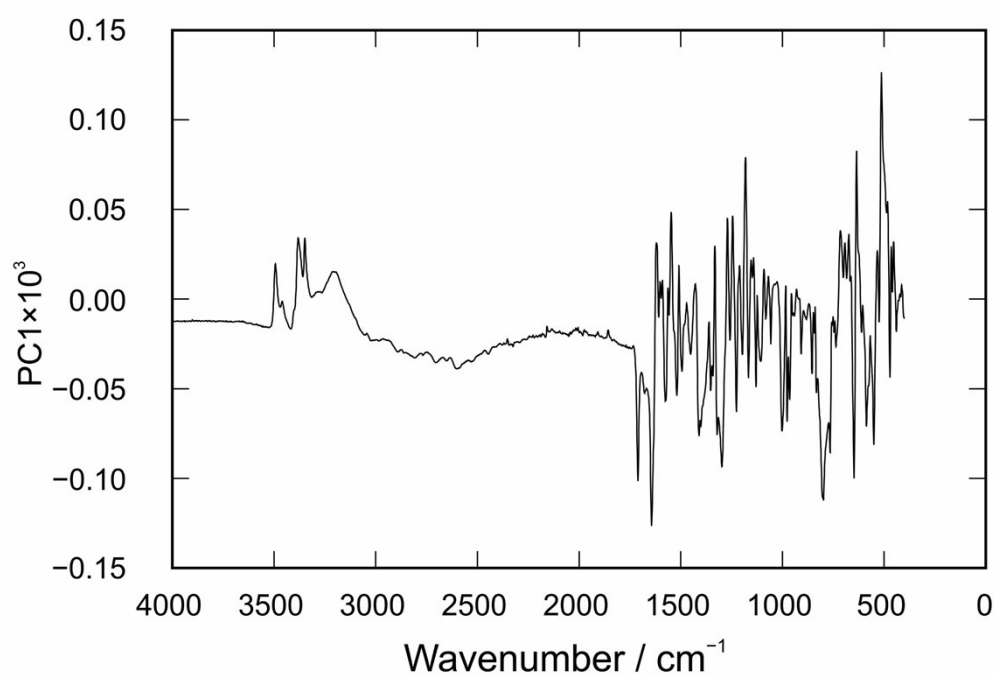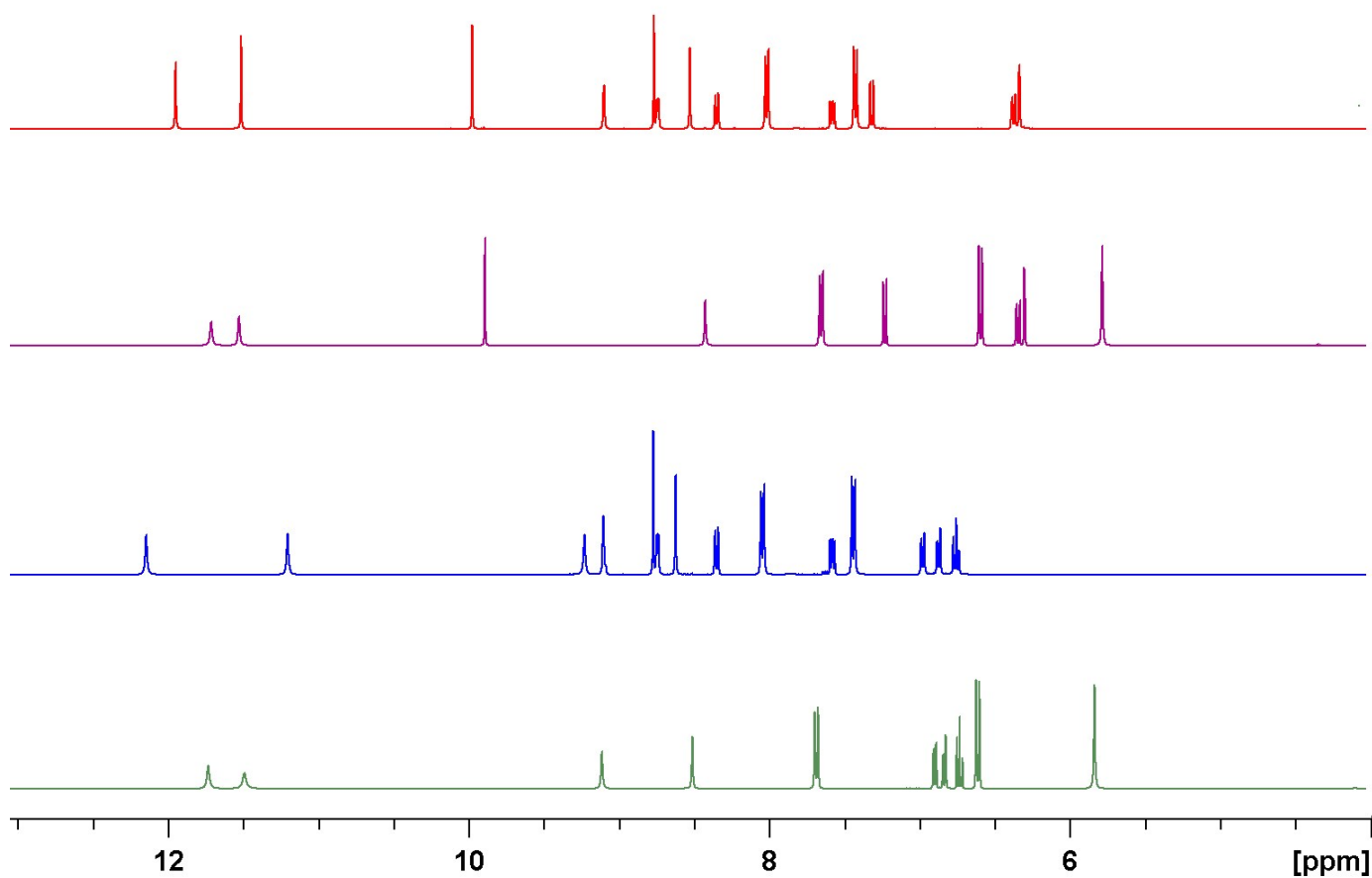

**Figure S26.** Principal component loadings calculated for a set of ATR spectra collected through vapour-mediated synthesis of **4b-4py.**

Figure S27. A comparison of the ^{1}H NMR spectra in dmso-d_6 of: **4a** (green), **4a-3py** (blue), **4b** (purple), and **4b-3py**. Singlets observed around 5.8 ppm, assigned to $-NH_2$ protons in the spectra of **4a** and **4b**, are missing in the spectra of the hydrazone-Schiff bases **4a-3py** and **4b-3py**.

**Table S8** ^{1}H and ^{13}C chemical shifts (ppm) of **5a** and **5b**.

Atom	5a		5b	
	δ / ppm (^{1}H)	δ / ppm (^{13}C)	δ / ppm (^{1}H)	δ / ppm (^{13}C)
11, 11'	-	118.90	-	110.75
12, 12'	-	147.87	-	161.15
13, 13'	-	146.14	6.34	102.94
14, 14'	6.96	119.35		162.54
15, 15'	6.79	119.91	6.41	108.68
16, 16'	7.14	121.76	7.42	133.42
OH	10.84 9.39	-	11.41 10.42	-
CH	8.97	163.87	8.78	162.23
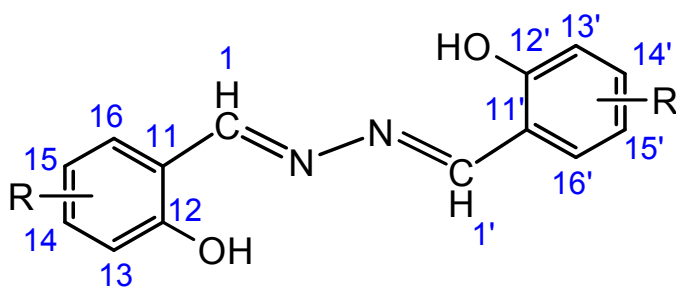
Figure S28. The structural formula of **5a** and **5b** with the NMR numbering scheme.
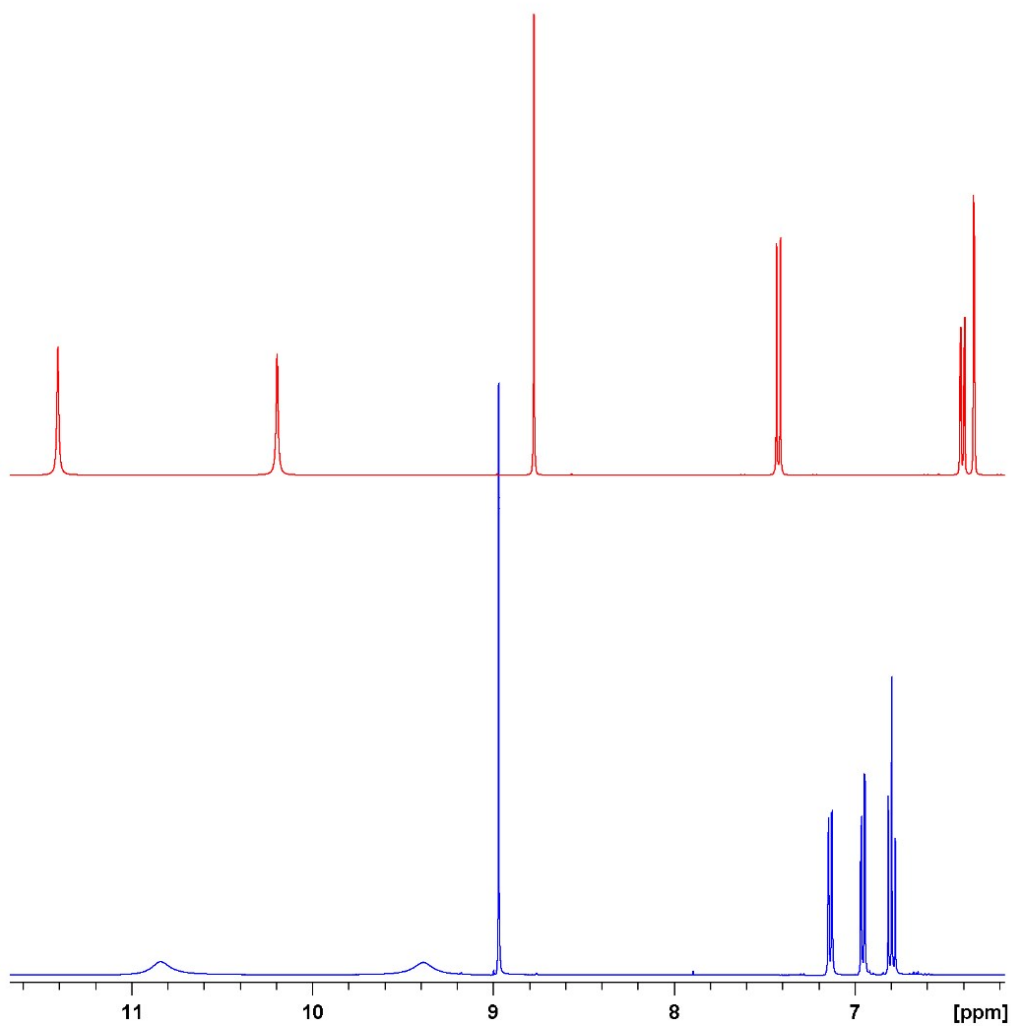
Figure S29. A portion of the ^{1}H NMR spectra in dmso-d_6 of: **5a** (bottom) and **5b** (top).
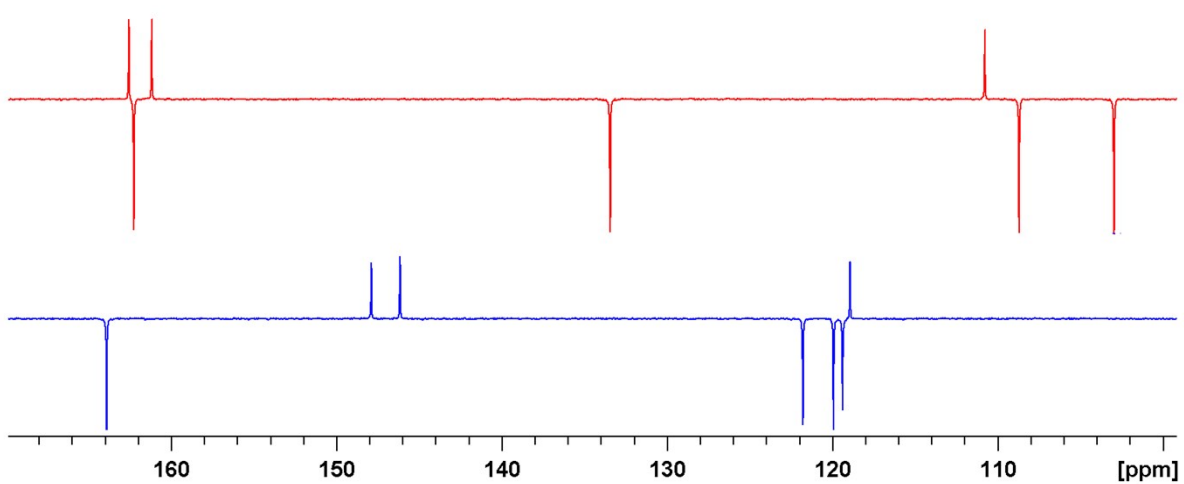
Figure S30. A portion of the ^{13}C NMR spectra in dmso-d_6 of: **5a** (bottom) and **5b** (top).

Table S9. *In vitro* cytotoxicity of the tested compounds.

Compound	IC$_{50}$/μmol L^{-1}	
	HepG2	THP-1
1a	>100	>100
1b	>100	>100
2a	>100	>100
2b	>100	>100
3a	>100	>100
3b	>100	>100
3c	>100	69.18
3d	>100	>100
4a	>100	>100
4b	>100	>100
4c	>100	>100
4d	>100	22.46
5a	>100	>100
5b	>100	>100
staurosporine	28.48	0.26

Table S10. *In vitro* antibacterial activity of the tested compounds.

Compound	MIC/μg mL^{-1}			
	S. aureus	*E. faecalis*	*E. coli*	*M. catarrhalis*
1a	>256	>256	64	16
1b	>256	>256	>256	32
2a	64	128	64	16
2b	>256	>256	>256	>256
3a	128	256	64	32
3b	256	>256	128	16
3c	256	256	64	8
3d	256	>256	256	16
4a	>256	>256	>256	16
4b	>256	>256	256	64
4c	128	256	64	8
4d	128	64	128	16
5a	>256	128	>256	8
5b	>256	128	>256	>256
azithromycin	2	8	0.25	0.25